Effects of Earth Encounters on the Physical Properties of Near-Earth Objects

by

Ho Chit Siu

Submitted to the Department of Earth, Atmospheric, and Planetary Sciences

in Partial Fulfillment of the Requirement for the Degree of

Bachelor of Science

at the

Massachusetts Institute of Technology

June 2014

Author _____

Department of Aeronautics and Astronautics

May 9, 2014

Certified by _____

Professor Richard P. Binzel

Thesis Supervisor

Certified by _____

Dr. Nicholas A. Moskovitz

Thesis Supervisor

Accepted by _____

Professor Richard P. Binzel

Chairman, Undergraduate Thesis Committee

Contents

Effects of Earth Encounters on the Physical Properties of Near-Earth Objects

by

Ho Chit Siu

Submitted to the Department of Earth, Atmospheric, and Planetary Sciences

in Partial Fulfillment of the Requirement for the Degree of Bachelor of Science at the Massachusetts Institute of Technology

Abstract

The effects of Earth encounters on the physical properties of near-Earth objects (NEOs) have been shown to be significant factors in their evolution. Previous studies have examined the effects of these encounters on reflectance spectra based on observational measurements, and effects such as spin state and shape changes have been studied for specific asteroids and through simulation. In this project, an automated light curve fitting routine was developed to support data reduction in an ongoing NEO survey. Additionally, data from previous NEO surveys were used to support simulation results by showing differences between encounter and non-encounter populations' rotational frequency distributions. These results demonstrate that Earth encounters have an effect on asteroid rotation by increasing the overall frequency as well as causing a wider distribution of frequencies when compared to non-encounter populations of NEOs. These data were, however, unable to show any effect on asteroid shape brought on by planetary encounters. A frequency comparison between NEOs that likely had Earth encounters to main-belt-equivalent asteroids did not show the same encounter effect, though the 'equivalent' asteroid populations were likely affected by a size/spin-rate bias.

Thesis Supervisors: Richard P. Binzel and Nicholas A. Moskovitz

Acknowledgments

I would like to thank my advisors, Rick Binzel and Nick Moskovitz, first for giving me the opportunity to write a thesis with them, and second for the support and guidance they have given throughout the process. They have been absolutely wonderful mentors, and have consistently helped push me in the right direction when I've been stuck at various parts of this project.

I would also like to thank Amanda Bosh for teaching me much of what I know about astronomy research, from setting up telescopes to data reduction, and for always getting us home in one piece after long observing nights.

Finally, I'd like to thank Jane Connor and Alissa Earle for helping me with the writing process and with polishing my presentations, and Alissa in particular for providing bananas.

Part I

Introduction

The study of the physical properties of asteroids is a key part of how we can understand the properties of the early solar system and how it formed. Asteroids represent a remnant of material left over from the early history of solar system formation which is largely unaffected by the various surface and internal processes that have altered the material that makes up the planets. However, this is not to say that the properties of asteroids have remained completely unchanged. Various gravitational and solar interactions experienced by asteroids have shaped the development of their properties over time (Bottke et al., 2002). The diversity of asteroid properties and orbits and how they have changed make it so that an understanding of the asteroid population serves as a proxy for us to study the formation and evolution of the solar system.

Near-Earth objects (NEOs) are a particularly interesting subset of the asteroid population. Earth encounters in particular can be a major contributor to the development of these objects if their orbits allow them to have such encounters. These encounters are known to affect the properties of NEOs through tidal effects. Binzel et al. (2010) showed that weathered surfaces of asteroids are 'refreshed' upon an Earth encounter, causing less reddening to be observed than would otherwise be expected. Richardson et al. (1998) conducted numerical simulations which showed that the tidal forces encountered by Earth-crossing asteroids may cause mass shifting and removal during flybys, resulting in changes such as distortions, and formation of fragment trains and orbiting ejecta. Rotation of the asteroid Toutatis was studied by Takahashi et al. (2013), who showed that there was a significant shift in rotational angular momentum during periodic Earth flybys.

To study asteroid properties such as rotation and shape, photometric light curves are measured, from which these properties may be extracted. A light curve is simply a plot of object brightness over time. The brightness variation (measured in astronomical magnitudes) seen in these light curves can vary due to changes in heliocentric and geocentric distance, rotation, aspect angle, and solar phase angle (Harris and Lupishko, 1989). The changes due to distance are generally removed during data reduction by using a 'reduced magnitude' value, but the periodic changes in brightness due to rotation and phase angle yield important information regarding the physical properties of the asteroid.

Rotational periods may tell us about the structure and collision history of an asteroid, while light curve amplitudes may tell us about the shapes of asteroids. Most larger asteroids (0.15 km $<$ D $<$ 10 km) are thought to be 'rubble piles' held together by self-gravity; a spin rate barrier appears to exist, because larger asteroids are not observed to spin faster than this 'barrier' rate (Pravec et al., 2002). As spin states asymptotically approach rotation around the principal axis of maximum moment of inertia, asteroid light curves are expected to be at least double-peaked, with the exception of near-spherical or other degenerate cases. Light curve amplitudes are indicative of asteroid shapes because elongated asteroids may have greater variation between the least amount of light that they reflect and the most that they reflect.

This thesis expands on the studies done on asteroid-Earth encounters by building a method for automatic light curve fitting from magnitude data and by examining the effects of Earth encounters on asteroid rotational periods and amplitudes — values that may be obtained from light curves. An automatic light curve fitting routine was developed for the ongoing Mission-Accessible Near-Earth Object Survey (MANOS), which began in the latter half of 2013. However, due to the timing of MANOS, there are not enough data produced by the fitting routine to support a significant analysis of Earth encounter effects. Therefore, data from the Jet Propulsion Laboratory

(JPL) and Minor Planet Center (MPC) were used in the analysis.

To approximate the probability of Earth encounters, the minimum orbit intersection distance (MOID) parameter was used. MOID is defined as the distance between the closest points of two bodies' osculating orbits. Here, MOID is a better parameter to use than the direct geometric distance between the Earth and the objects because the integration of an object's position in its orbit loses precision much faster than information about the orbit itself. This difference in loss of precision lends greater value to using MOID for timescales on the order of centuries or more. It is important to note, though, that MOID provides an estimate of the lower bound of the distance of an encounter. It does not guarantee that an encounter occurs, but simply suggests an increased likelihood with a lower value. Instantaneous MOID may be determined from the present-day orbital parameters of an object, and was used here to look at the relationship between encounters and period/amplitude.

Part II presents the background of NEO populations, the effects of planetary encounters on NEO rotational dynamics, and describes past and current asteroid surveys. Part III presents the automatic light curve fitting software developed as part of this project, particularly tailored for the ongoing nature and specific targets of MANOS. Part IV presents the results obtained from the Earth encounter analysis of the NEO population. Finally, Part V introduces future work that can be done to follow up on this project.

Part II

Background

To motivate the work done for this thesis, Part II provides a broad description of the NEO population and its significance within planetary science. Additionally, previous work on various effects of planetary encounters is reviewed, along with a brief discussion of the asteroid surveys that produced much of the data used in studies of NEOs.

1 The NEO Population

Asteroids, comets, and large meteoroids whose orbits intersect or nearly intersect Earth's are classified as Near-Earth Objects (NEOs). These objects are typically divided into three major categories based on their orbital elements: the Aten, Apollo, and Amor groups, which are collectively known as the AAA asteroids (Shoemaker et al., 1979). Atens are defined as objects having a semimajor axis $a < 1.0$ and an aphelion distance $Q \geq 0.983$ (the perihelion distance of Earth). This classification means that Aten objects only sometimes cross the orbit of Earth. Apollos are defined to have an $a \geq 1.0$ and a perihelion distance $q \leq 1.0167$ (the aphelion distance of Earth); Apollos also cross the orbit of Earth. Amors are defined solely by their perihelion distance, namely $1.1067 \leq q \leq 1.3$, meaning they are near-Earth-crossers but do not currently qualify as Earth-crossing asteroids. An NEO is considered a potentially hazardous object (PHO) if its minimum orbit intersection distance (MOID) is less than 0.05 astronomical units (AU) and has an absolute magnitude of 22.0 or less (JPL, 2014a). Orbital perturbations may, of course, change the classification of any particular NEO between these groups.

The orbital characteristics of NEOs generally mean that they stay as NEOs for

at most a few million years, eventually crashing into the Sun or terrestrial planets, or being flung out of the solar system (Binzel et al., 2002). The fact that the number of NEOs has remained steady over the last 3 billion years suggests that there is a source of resupply for the population (Bottke et al., 2002). It is believed that main belt asteroids (MBAs) provide the bulk of NEO resupply, with Jupiter and Saturn resonances causing asteroids to move from main belt to NEO orbits. Smaller NEOs are likely collision fragments from MBAs, and exhibit younger (less-weathered) surfaces due to the difficulty of surviving further collisions or planetary encounters (Binzel et al., 2002). Additionally, about 5% to 10% of NEOs may be extinct comets (DeMeo and Binzel, 2008).

The NEO population is of special interest to planetary astronomers because of its proximity to Earth. NEOs with low inclination and low eccentricity in particular are some of the best solar system targets for space missions due to the relatively low ΔV (a measure of the amount of propulsion required to change trajectories) and short time frame required to reach them. Additionally, the inner-solar-system orbits and periodic proximity to Earth of these NEOs mean that thermal and power considerations for rendezvous and flyby missions can be significantly simplified compared to near-Sun or outer-solar-system missions, making them relatively low-cost and within the reach of early private-sector space missions (Perozzi et al., 2001).

2 Planetary Encounters

Tidal forces encountered near planets can cause a number of changes to asteroids. Distortion and disruption have been found to occur with Earth-crossing asteroids in numerical simulations, with results ranging from elongation and mass stripping, to the formation of fragment trains and binary systems. Low-inclination, low V_∞, and long-rotational-period asteroids experienced the most severe effects in these simula-

tions (Richardson et al., 1998, Bottke et al., 1998). Chapman (1978) argues that large, monolithic MBAs may have been fragmented by collisions to form rubble piles. The lack of observed fast-rotating asteroids with absolute magnitudes $H < 22$ suggests that larger NEOs are indeed such rubble piles and have minimal tensile strength, where any additional spin-up would cause disruption (Pravec and Harris, 2000). Smaller NEOs, however, may remain monoliths due to the fact that they were spun off from these rubble piles and have already experienced forces that would disrupt them if they were rubble piles. Fragment trains are generally formed from distortion processes that cause elongation, resulting in a pattern similar to what happened to Comet D/Shoemaker-Levy 9 during its 1992 Jupiter encounter (Shoemaker et al., 1979). Binary systems, on the other hand, are often formed from spin-up, which causes rubble-pile asteroids to fling mass off their equators, resulting in an orbiting body (Pravec and Harris, 2000, Pravec et al., 2002, Walsh and Richardson, 2006).

Planetary encounters have also been shown to cause 'freshening' of the surface of asteroids. This process runs counter to the usual 'space weathering' process whereby asteroids become increasingly reddened. Binzel et al. (2010) showed that Earth-crossing asteroids that have closer encounters with the terrestrial planets tend to appear less weathered. This investigation involved using the Minimum Orbit Intersection Distance (MOID) parameter as a measure of the possibility of an Earth encounter, showing that for an integrated MOID, objects that likely had planetary encounters over the past 500,000 years showed less signs of weathering than objects that were kept away from a planetary encounter (perhaps by orbital resonance) (Binzel et al., 2010).

Numerical simulations across a distribution of asteroid spin states showed that while planetary encounters may cause spin-up, spin-down, or tumbling in individual asteroids, there is an overall trend towards spin-ups, one that is particularly prevalent

for bodies with a slow initial rotation (Scheeres et al., 2004). Tumbling cases may be created only if the flyby occurs out of the asteroid's equatorial plane, as gravitational forces along the plane would at most cause a spin-up or spin-down (Scheeres et al., 2000).

Recently, radar imaging of 4179 Toutatis — an asteroid that makes periodic near-Earth flybys — gave a series of observations that showed terrestrial tidal torques altering the rotational dynamics of the asteroid. These torques mostly caused changes in orientation as the asteroid passed close to the Earth, but a particularly close encounter in 2004 demonstrated a significant perturbation in the angular momentum of the asteroid that persists to the present (Takahashi et al., 2013).

Thus, it may be seen from the literature that planetary encounters play a major role in the evolution of near-Earth objects that experience such effects. These effects have been studied in detail in simulation for a range of encounter situations. Additionally, they have also been seen in observations of individual asteroids, as well as in groups of asteroids through data from large-scale asteroid surveys.

3 Asteroid Surveys

Large-population studies of NEOs have drawn primarily from the data produced by large-scale asteroid surveys. Within the past decade, new technologies have shifted the observing focus of these surveys from larger, multi-kilometer-sized MBAs and NEOs to smaller sub-kilometer-sized NEOs. Asteroid surveys in the past have been able to find and characterize thousands of main-belt and near-Earth asteroids. Many past surveys focused on discovery, with examples including LONEOS, LINEAR, Catalina, and Pan-STARRS. Some studies were specifically for characterization of known objects, such as the albedo characterization done by IRAS, WISE and Akari, and the spectral characterization done by SMASS. These surveys were able to exten-

sively sample the population of asteroids that are larger than the rubble pile limit; however technological limitations meant that they were biased towards being able to observe larger, brighter objects, rarely being able to resolve asteroids dimmer than 22nd absolute magnitude (Binzel et al., 1989, Jedicke et al., 2002, Stokes et al., 2002).

The past decade has seen a rapid increase in the number of NEO detections, partly due to advances in observation and computing technologies, but also because of increased urgency started by a mandate by the American government to characterize 90% of NEOs larger than 1 km that may present an impact hazard to Earth (Binzel et al., 2002, Morrison, 1992). A new, multi-year program started in August of 2013 called the Mission Accessible Near-Earth Object Survey (MANOS) seeks to leverage advances in observing capabilities to characterize asteroid targets that are more than an order of magnitude smaller than those covered by previous studies. Using telescopes such as Gemini, SOAR, Kitt Peak 4m, and CTIO, MANOS is specifically focusing on sub-kilometer-sized targets that would be accessible by space missions utilizing conventional chemical propulsion, providing rough characterization of targeted NEOs via astrometry, light curves, and spectra. 'Mission-accessible' is defined as having a $\Delta V < 7$ km/s, which is the approximate limit of conventional chemical propulsion.

The program aims to characterize approximately 100 NEOs per year, meaning that there will be a large throughput of data during the survey period, which is expected to last 3 to 5 years. Part of the work done for the thesis was development of automated data processing software for the MANOS pipeline. Automation for MANOS is particularly useful due to the volume of data that will be generated by the survey. Automatic data processing serves to free up manual processing time, as well as to increase consistency in how results are produced over the course of the survey period.

Part III

Light-Curve Fitting

The automation work done for this thesis focused on light-curve fitting for the photometric data produced by MANOS. To automate this processing, a fitting routine, manosCurveFit, was developed by the author to automatically scan reduced MANOS photometry data and fit them to a light curve model which provides the period and amplitude. Before this work, curve fitting for MANOS was done using software built using MATLAB, which contained some components that were relatively poorly documented and required a proprietary platform. Other common fitting methods, such as Canopus, were similarly based on proprietary software. manosCurveFit was developed from scratch specifically for the MANOS data pipeline; it represents one of very few pieces of light curve fitting software that is free and open source, and possibly the only such software that is tailored for asteroid fits.

1 Software Details

1.1 System Overview

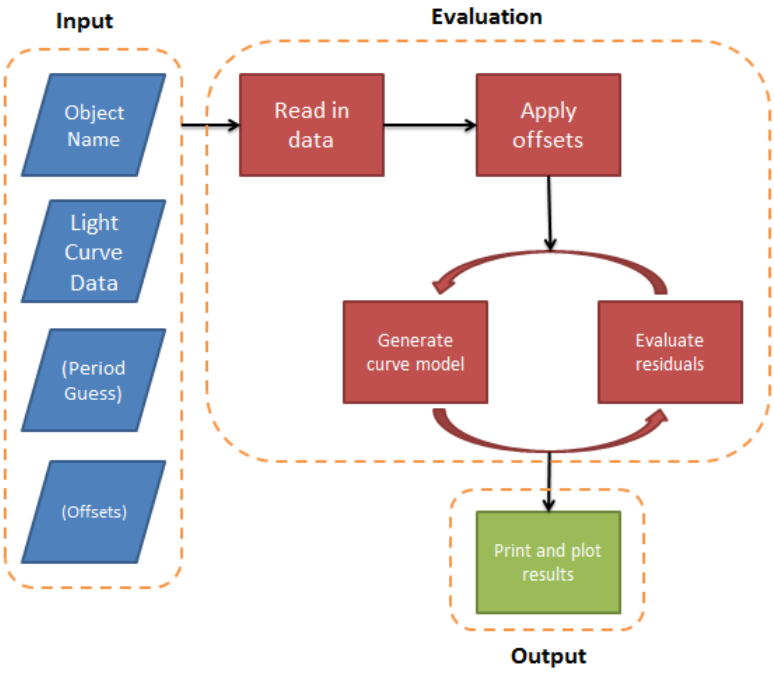

Figure 1: Flowchart showing the conversion from raw data to fitted plots.

In order to find a the most likely period and amplitude of a light curve given photometric data from an asteroid, the fitting routine fits a mathematical model of the photometric variation to the light curve data. The fitting process may be generally divided into input, evaluation, and output portions. The inputs in parentheses are not required for the fitting to work, but a guess at the rotational period may significantly constrain the search space, and if data are taken over multiple nights and/or by different instruments, offsets are required to normalize the magnitudes to some baseline. A number of other inputs may also be supplied to constrain or expand the search space. These inputs may be supplied by the fitInfo file for each object. The light curve data are then read in from one or more text files with standardized columns.

Once the raw data and the fitting parameters have been read in, two kinds of magnitude offsets are applied: offsets by night/instrument, if provided, and a normalizing offset which subtracts the weighted average magnitude of the set from the entire set. The normalizing offset is necessary in order to center the data points on the y-axis for fitting purposes, and may be used in this context because only differential magnitudes are needed. These offsets act as a coarse adjustment for y-axis centering. A finer adjustment is made by a y-axis offset for the model, which is taken to be part of the least squares minimization. For each period to be checked, a least squares minimization is performed for each order of Fourier coefficients from two to six, unless specified otherwise in the fitInfo file. The parameters that generate the best fit to the data are kept and printed at the end, along with the light curve and residual plots.

See the Appendix for further software documentation.

2 Fitting Rationale

The fitting routine used by manosCurveFit is based on equations 1, 2, and 3 from Harris and Lupishko (1989) (corresponding to equations 1, 3, and 4 respectively, below), which describe the fitting model for a light curve, the residuals of the model, and the bias-corrected variance, respectively. The fitting model is described by the Fourier Series

$$H(\alpha,t) = \bar{H}(\alpha) + \sum_{L=1}^{m} A_L sin\frac{2\pi L}{P}(t-t_0) + B_L cos\frac{2\pi L}{P}(t-t_0). \quad (1)$$

$\bar{H}$ is a correction to get the absolute magnitude of the asteroid. Absolute magnitude is defined to be the visual magnitude of an asteroid if it were at zero phase angle and at 1 AU from both the Earth and the Sun, which, in combination, is actually a set of unphysical conditions (JPL, 2014b). Here, $\bar{H} = 0$ because absolute magnitudes

are not necessary for MANOS, and m (the series order), P (the period), and A_L and B_L (the Fourier coefficients) are free parameters. Since a fine-adjustment y-shift is also added, the actual fitting equation becomes

$$H(\alpha, t) = y + \sum_{L=1}^{m} A_L sin\frac{2\pi L}{P}(t - t_0) + B_L cos\frac{2\pi L}{P}(t - t_0), \tag{2}$$

where y is an additional free parameter, which generally takes on a small value.

The residual of a particular observation i may be obtained by

$$\frac{\delta_i}{\epsilon_i} = \frac{V_i(\alpha_j) - H(\alpha_j, t_i)}{\epsilon_i}, \tag{3}$$

where α_j is the reference phase angle on the j^{th} night, t_i is the time of the i^{th} observation, and ϵ_i is the error of the measurement. In the context of NEOs, the phase angle may very well change, particularly as targets pass very close to Earth. However, the majority of MANOS targets will be observed for a short period of time (on the order of a few hours) and characterization of these targets will be done solely on the basis of a one-time observation. Therefore, α will be assumed to be a constant due to the time scales involved in the single observation, and as such, manosCurveFit does not take phase angles into account. The least squares minimization is then performed on the bias-corrected variance, given by

$$s^2 = \frac{1}{n-k}\sum_{i=1}^{n}\left(\frac{\delta_i}{\epsilon_i}\right)^2 = minimum, \tag{4}$$

where n is the total number of observations, $k = 2m + 1$, where m is defined in 1. The total number of nights of data is also added into k in the form that Harris et al. use, but here, this again needs not be considered because we are concerned with differential photometry, and offsets for different nights will be provided as necessary.

By default, the program will run the fit from $m = 2$ to $m = 6$. The minimum of order two is due to the fact that asteroid light curves are expected to be

double-peaked (except for some cases of complex rotation or degenerate cases of near-spherical bodies), and the maximum of order six is used to prevent over-fitting. The curve is centered around zero magnitude by a weighted average of the data, but since there is often still a slight magnitude offset due to the nonuniform nature of the sampling, a magnitude offset parameter was added to allow for a better fit. The user does not normally interact with the optimization of this y-shift parameter.

Precautions were taken to prevent over-fitted or unsubstantiated models. Any models which produce amplitudes greater than 2 were automatically rejected. This is necessary to prevent the fit from assuming a model in which the data are a small portion of a much longer period with one or more large spikes where data are not present. As an additional precaution, if the fitted period is more than 25% of the range of the phase-folded data points, a warning is given to notify the user of a potentially under-constrained model.

3 Fitting Results and Data Products

By default, the software automatically produces two figures and a text file report of the fit, which are then saved to the same folder as the data. Examples of these for plots may be seen in Figures 2 and 3. The bottom sub-plot of Figure 2 is an optional plot which shows the residuals of the generated fit. This plot may be used as an additional manual check on the fit by seeing if any structure or bias remains in the residuals, which may indicate that a higher-order fit is required. Additionally, any significant magnitude bias in the residuals plot may be indicative of an incorrect offset of a particular night, if multiple nights' data are used (this effect should also be visible in the main fitted plot). Figure 3 shows the root mean square (RMS) values of different periods that were attempted during the fitting process, with the fit that provided the minimum RMS value representing the one that was eventually

accepted. These figures represent a set of data that was composed of 12 nights, split into two input text files, all of which were automatically merged and processed by the program. This kind of dataset is more complex than most typical MANOS datasets, which will generally be data from a few hours on one instrument for a single night, so multiple input files and automatic merging will largely be unnecessary for the usual MANOS application.

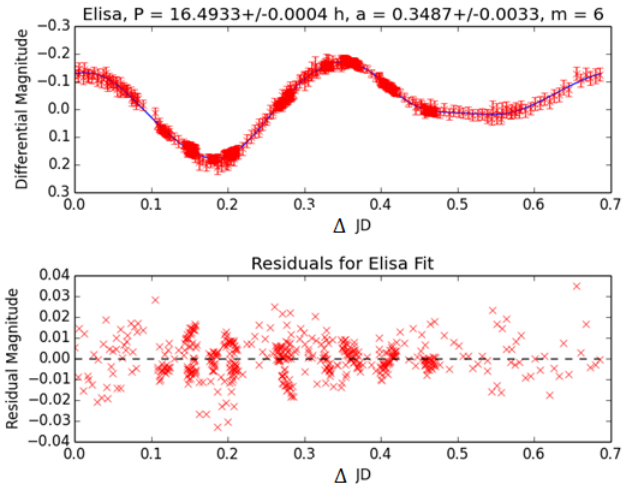

Figure 2: One of the figures produced by manosCurveFit, showing the data points on top of the fitted model (top) along with the residuals of the fit (bottom). The model automatically phase-folded the data to give the best fit, and the residuals here show an example of what would occur for a good fit, since there is no notable bias or structure in the residual plot. The residuals plot shows a line at zero magnitude to help in finding any structure or bias.

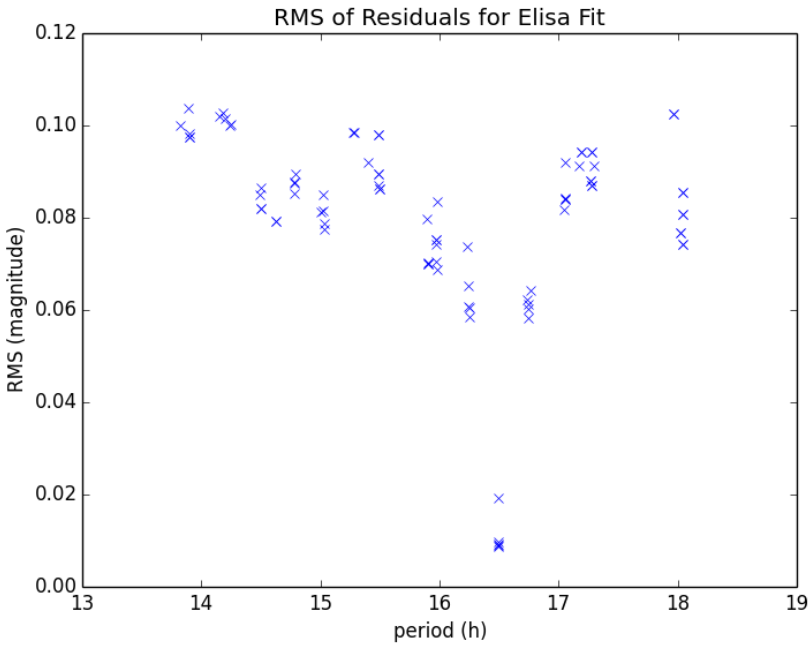

Figure 3: The second figure produced by manosCurveFit, showing the mean RMS values of the fit when different periods were attempted.

The fitting routine was tested against five objects with varying light curve structures, three of which had previously-determined periods. Table 1 shows the comparison between the fitted and accepted periods of the latter three objects, all of which showed very low error values (if any), even though the data used for the fit is only a small subset of the entire set of data used to generate the accepted period. 2579 Spartacus had a different fitted period than accepted period likely due to the fact that the accepted period is based on a much larger baseline of data than what was used for the fit.

Table 1: Period comparisons between fit and accepted values.

Object	**Fitted Period (h)**	**Accepted Period (h)**	**Error**
2012 DA_{14}	5.95 ± 0.12	5.8 ± 0.3	consistent
956 Elisa	16.4933 ± 0.0004	16.494 ± 0.001	consistent
2579 Spartacus	3.812 ± 0.019	3.63599 ± 0.00004	4.84%

Part IV

Analysis of Physical Properties with Respect to Earth Encounters

NEO orbital and light curve parameters from JPL's Horizons database and several Minor Planet Center databases were used to examine the physical properties of NEOs with respect to Earth encounters. Minimum orbit intersection distance (MOID) was used as a proxy for Earth encounters, as lower MOID values indicate a higher likelihood of a near-Earth flyby. Magnitude, rotational frequency, and light curve amplitudes were examined in relation to MOID values, and attempts were made to show a difference (or lack thereof) in these properties between NEOs that had Earth encounters and those that did not.

1 Overview and Hypothesis

NEO light curve frequencies, light curve amplitudes, and absolute magnitudes were compared to their MOID values. Data analysis sought to find differences in the distribution of these values over selected subsets, leveraging the aggregated values of groups of NEOs to look for trends in the overall data. Since MOID presents only a lower bound of the actual intersection distance, a small MOID does not guarantee that an object actually passed near the Earth, but rather only increases the likelihood that it did. A trend in the properties of the distribution within these groupings with respect to MOID would be a possible indicator an Earth encounter effect. The focus of the comparison is between objects that may have had an Earth encounter and those that have not. A rough boundary for a MOID that is indicative of a possible Earth encounter is a value of <0.0026 AU, or <1 lunar distance (LD), though populations

with somewhat higher MOID values may also display encounter characteristics, so a larger range was checked. The details for how this was done may be found in the Results section.

Based on the literature review presented in Section 2 — particularly the simulations of Earth encounters done in Scheeres et al. 2000 and Scheeres et al. 2004 — it is hypothesized that a population of objects that have undergone a planetary encounter will likely have greater variation in rotational period and amplitude. This variation is, however, unlikely to be pronounced, as the limitations of MOID mean populations with some, but not all, objects that have had some Earth encounter are the best that can be selected. Again noting the simulations done by Scheeres et al. (2004), it is hypothesized that the analysis may show a slight spin-up in objects that have had planetary encounters. It is likely that this effect will also prove difficult to show (perhaps showing possible statistical significance in some cases, and no statistical significance in the rest) because the simulations showed that spin-up is a prominent effect only in asteroids with initially slow rotations, and asteroids with initially slow rotations cannot be distinguished in the data being used.

This analysis will make two primary comparisons: within the NEO population, and between the NEO population and the Main Belt Asteroid (MBA) population. In both cases, the comparison will be made between a group that is suspected to have had an Earth encounter and a group that has not. The NEO/MBA comparison in particular was made to check NEO characteristics against a population of asteroids that is essentially the most 'pristine' in the solar system — meaning that they are among the least gravitationally perturbed asteroids, and almost certainly have not had any close planetary encounters.

2 Description of NEO Data

Two main sources of data were polled for the analysis done in this project. The Jet Propulsion Laboratory's (JPL) Horizons database was polled for MOID, magnitude, and rotational period; it did not contain light curve amplitude information. Two databases were taken from the Minor Planet Center (MPC) — one of light curve and one of NEOs — and combined to obtain MOID, magnitude, rotational period, and amplitude information. The MOID values from both sources were instantaneous MOIDs calculated from the present-day orbital elements. For NEOs, the Horizons dataset contained 10938 objects, 10775 of which contained both magnitude and MOID information, 685 of which contained both rotational period and MOID information, and 680 of which contained all three. For MBAs, the Horizons dataset contained 577438 objects, 574200 of which contained magnitude information, and 573105 of which contained both magnitude and period information. The analysis done for rotational frequency (calculated from the rotational period) was done using the Horizons data.

The MPC's NEO datasets contained information for 827 Aten, 5306 Apollo, and 4500 Amor objects when it was polled for this project in March of 2014, while the light curve database contained 2326 objects. The light curve database had the amplitude and period information for each object, but lacked MOID data, which was contained in the NEO dataset. As such, it was necessary to merge the two sets, cross-referencing objects contained in both to obtain a complete listing of light curve properties and MOID. The resulting set contained 274 objects, of which 245 contained amplitude, magnitude, and MOID information (29 objects did not have amplitude values despite being in the light curve database). Since this dataset contained light curve amplitude values, it was used for the amplitude analysis.

The breakdown of the number of objects used for this analysis is presented in Table 2.

Table 2: Breakdown of NEO data sources.

JPL Horizons NEO Database (10938 NEOs total)		
NEOs that have	MOID	10938
	MOID + magnitude	10775
	MOID + magnitude + period	680

JPL Horizons MBA Database (577438 MBAs total)		
MBAs that have	magnitude	574200
	magnitude + period	573105

MPC NEO Database (2326 NEOs total)		
NEOs that have	MOID	274
	MOID + amplitude + magnitude	245

3 Results

The results of comparing three asteroid properties to MOID values are presented in this section. Magnitude is presented briefly as a property that does not have a physical significance in relation to MOID, but which has a biasing effect for other properties that must be considered. Rotation frequency and light curve amplitude are then presented. Debiasing procedures are described for the latter two properties, and the binning method used to compare NEO populations that have had encounters to those that have not are presented. Finally, the results of statistical testing to examine differences between encounter and non-encounter populations are presented for both rotation frequency and light curve amplitude.

3.1 Magnitude Analysis

The absolute magnitude (H) was plotted against the MOID of the objects. On the semi-log plot shown in Figure 4, it can be seen that objects with higher H values tend to have lower MOIDs, which fits with the observational bias of being more likely to

see dimmer objects if they pass closer to Earth.

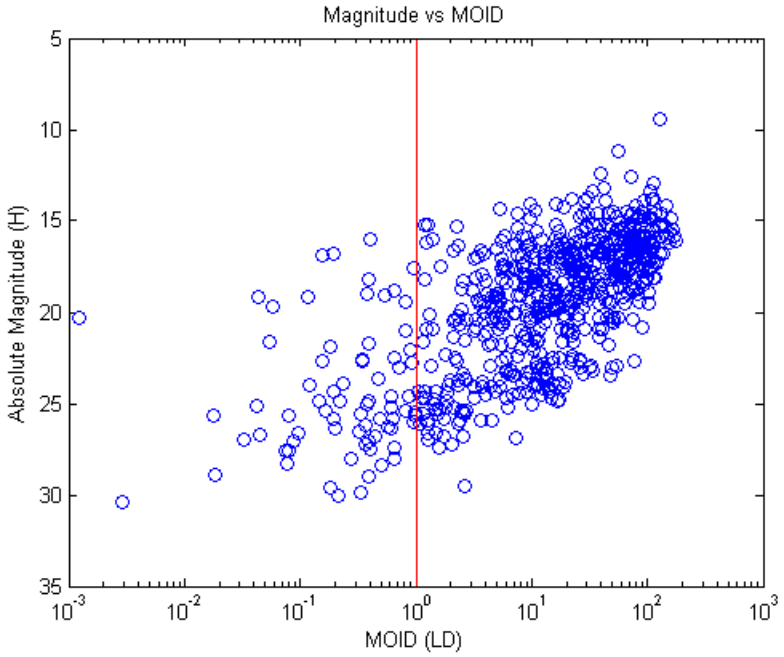

Figure 4: Semi-log scatterplot of absolute magnitude against MOID. The plot shows a correlation where dimmer (smaller) objects tend to have lower MOID values. The red line represents 1 LD.

3.2 NEO Rotation Frequency Analysis

As an initial examination of various possible effects on rotation frequency, frequency was plotted against MOID (Figure 5) and absolute magnitude (Figure 6).

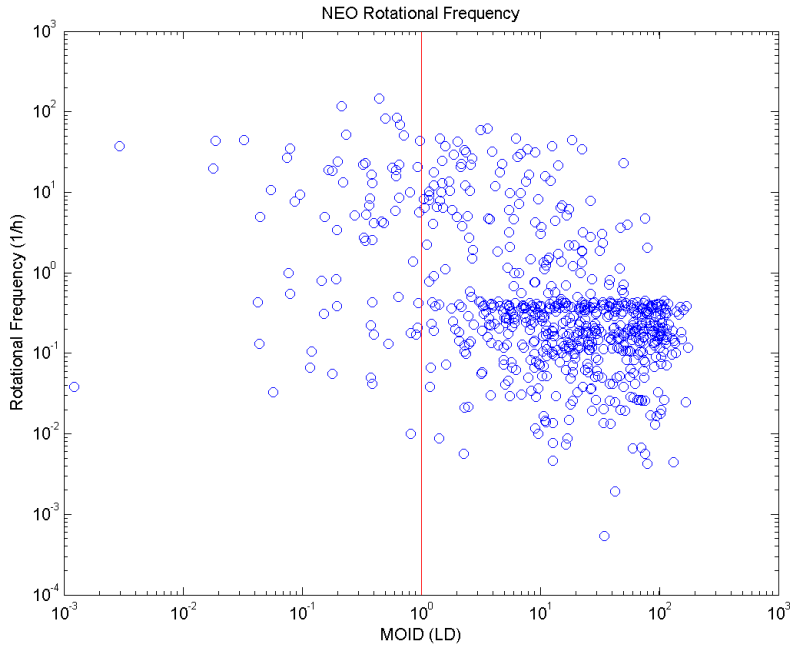

Figure 5: Frequency vs. minimum orbit intersection distance for Aten, Apollo, and Amor (AAA) NEOs. The red line represents 1 lunar distance (LD). Debiasing and analysis of these data are presented in this section.

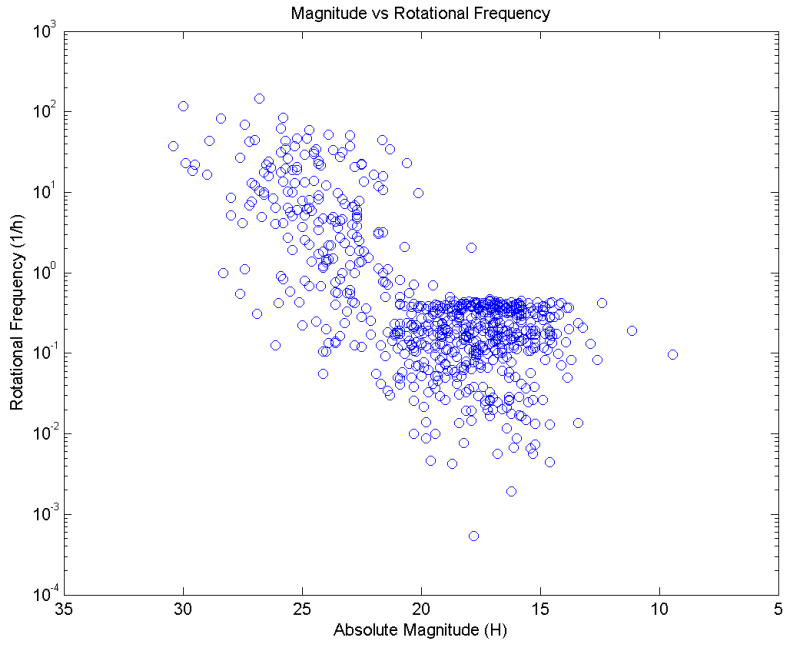

Figure 6: Plot of absolute magnitude against rotational frequency. Higher-magnitude (smaller) objects tend to have faster rotations.

A 30-window moving-average plot was then used to examine the mean and standard deviation of frequency as a function of MOID, as shown in Figure 7. It should be noted that for moving average plots such as this, consecutive mean and standard deviation values are not independent, and independence of these values only occurs for points that are at least one window apart (i.e. points that have at least 30 other points between them).

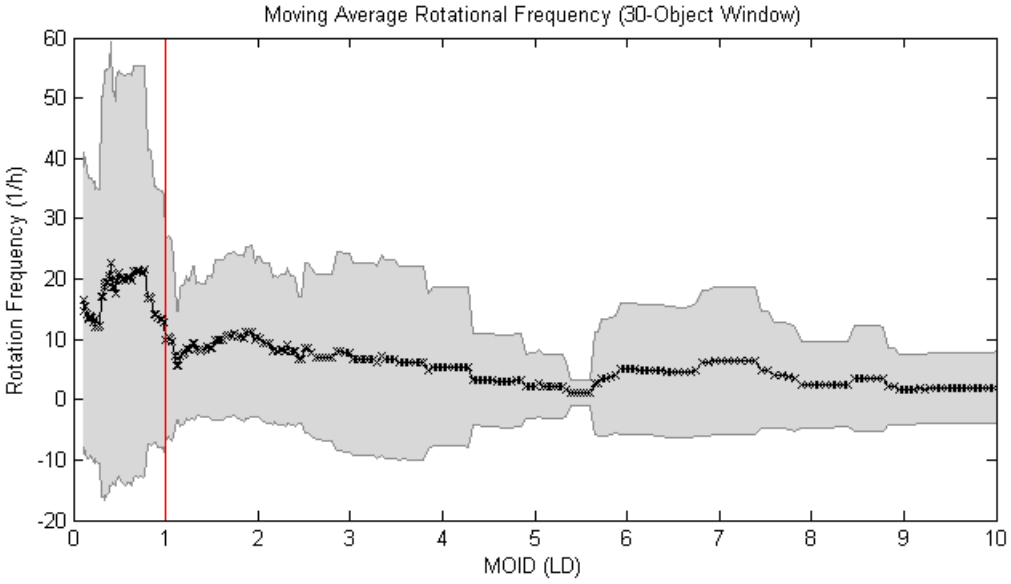

Figure 7: Moving average plot of rotational frequency (without bias correction) with a 1-LD reference line. Each 'x' mark represents the mean MOID of one 30-object window, and the shaded region represents one standard deviation of the mean above and below the mean value. Note the higher standard deviation in the population with MOID $<$ 1 LD.

However, it may be seen from Figure 6 that objects that have higher magnitudes (likely to be smaller objects) tend to display faster rotations, which is consistent with the asteroid collision evolution model predicted by Chapman (1978). This bias makes the result given by Figure 7 less reliable, since it is likely to be affected by the fact that dimmer asteroids are more likely to be observed closer to Earth (Figure 4), and these dimmer asteroids are likely to be smaller and therefore have

higher rotational frequencies (Figure 6). In order to better examine the distribution of rotation frequencies as a function of MOID, a correction must be made for this size/rotation bias. Thus, when analyzing the frequency distributions, only objects within a certain range of magnitudes were compared to each other. To select an appropriate window of magnitude values to conduct this analysis over, Figure 6 is first referred to in order to pre-select a range of magnitudes that provide a sufficient spread of frequencies. It may be seen from the figure that objects brighter than 20th magnitude do not have a very wide range of frequencies, which restricts the range to be analyzed to objects dimmer than 20th magnitude. From this sample, it can be seen from Figure 8 that there is likely still some size/rotation correlation. Thus, a further step is needed to select a bias-free sample.

To down-select even further to get a sample of asteroids that is free of the size/rotation bias, a search procedure was conducted over the magnitude space. The space was discretized into 0.5-magnitude steps, and an exhaustive search across all possible continuous subsets of this space was conducted to look for subsets that do not contain a significant magnitude/frequency correlation. Of the subsets that did not contain a magnitude/frequency correlation ($p > 0.15$) , the largest subset was kept and used as the window for analysis. The black lines on Figure 8 show the final window that was selected (from 24.5 to 29.5 magnitude).

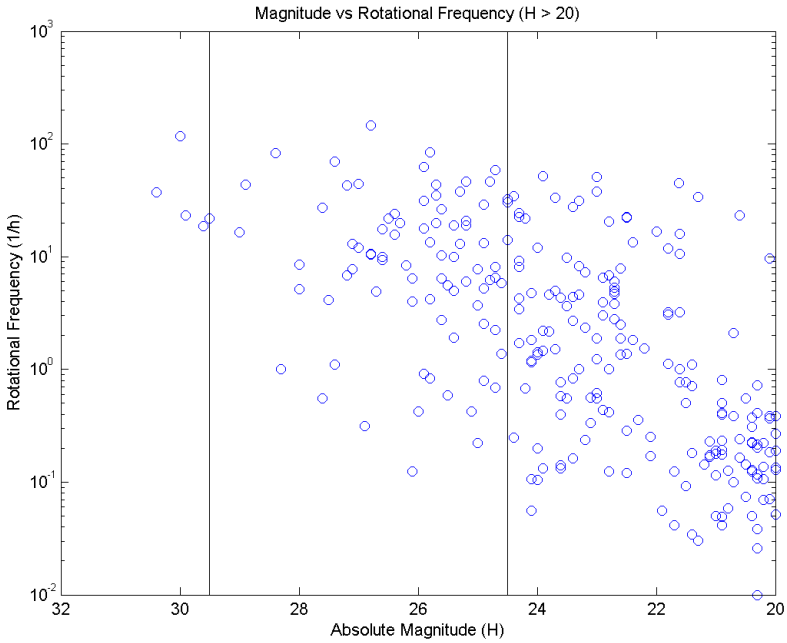

Figure 8: Plot of absolute magnitude against rotational frequency for objects of magnitude > 20. This magnitude range was preselected due to the number of objects and the range of rotational frequencies represented in it. From this sample, the subset between the black lines (24.5 to 29.5 magnitude) was then selected for analysis due to its lack of magnitude/frequency correlation.

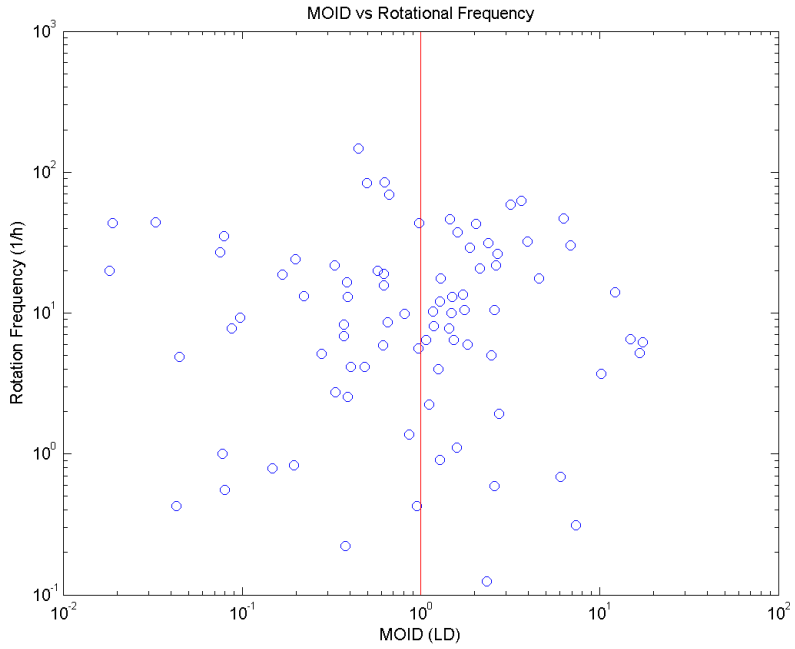

Figure 9: Comparison of the MOID vs rotational frequency distribution for objects ranging from magnitude 24.5 to 29.5 magnitude.

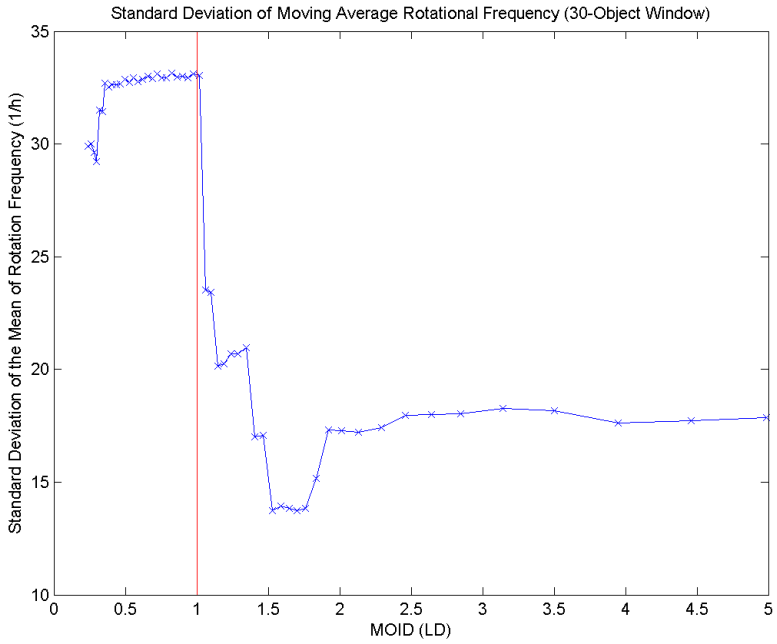

Figure 10: Plot of standard deviation of the mean of 30-object samples of objects in the magnitude range from 24.5 to 29.5 LD. Points are placed along the x-axis according to the mean MOID values of each 30-object set. A 1-LD line has been inserted for reference.

Next, a two-sample one-tailed Student's t-test was conducted to see if there was a statistically significant difference between the means of the rotational frequencies of objects in the MOID range where planetary encounters are possible and other MOID ranges, specifically if the frequencies in the group that had smaller MOID values were greater than the frequencies of the group with larger MOID values. Similarly, a two-sample one-tailed f-test was conducted to see if there was a statistically significant variance between the rotation frequencies of different populations, specifically if the variance of the frequencies in the group that had smaller MOID values was greater than the variance seen in the group with larger MOID values. The two samples for each test were binned according to a dividing MOID value, for which one sample ranges from 0 to the dividing MOID, and the other ranges from the dividing MOID to the maximum MOID value in the data set (174 LD). Dividing MOID values were chosen to range from 1 to 10 LD. This range of dividing values was chosen because

objects with low MOID are more likely to have experienced some sort of encounter, and the probability of past encounters goes down with increasing MOID. An example of how the binning was done may be seen in Figure 11.

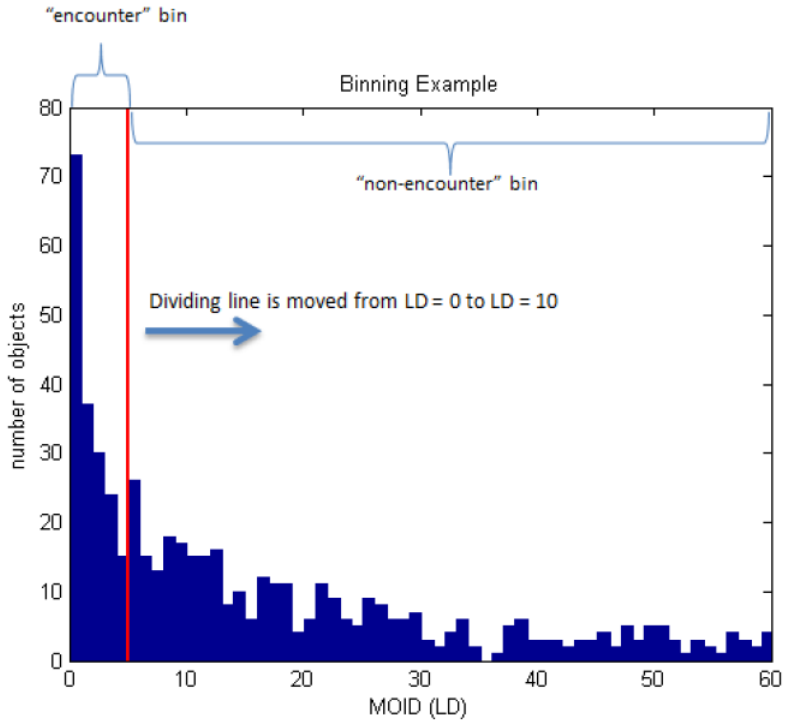

Figure 11: Example of how the dividing line and the two-bin system works. The histogram is used for illustration only, and does not reflect the data that was selected for use in this analysis.

A summary of the statistical tests are shown in Table 3. The results of the t-tests and f-tests are also shown graphically in Figure 12, where p values lower than 0.1, 0.05, and 0.01 represent possibly significant, significant, and highly significant differences between the two samples.

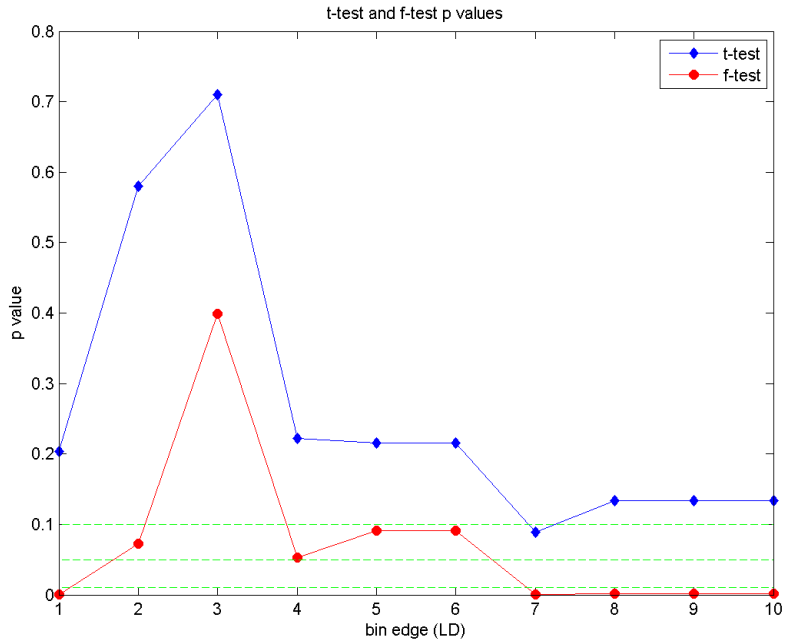

Figure 12: Results of one-tailed Student's t-tests, and one-tailed f-tests conducted for rotational frequencies. Dashed lines represent p values of 0.1, 0.05, and 0.01, respectively.

3.3 NEO vs MBA Rotational Frequency Comparison

In addition to the frequency analysis done for the NEO population, a second analysis was done comparing the 'encounter' subset of NEOs to equivalent main belt asteroids. This analysis was done to test the hypothesis of the effects of encounters on frequency against a population that almost certainly did not have any sort of Earth encounter. Since the main belt is believed to be the source of NEOs, we may reasonably treat the MBA population as a 'pre-disturbed' version of the NEO population for the purposes of this comparison (Bottke et al., 2002). The magnitude-frequency bias noted in the NEO analysis still holds here, so certain restrictions must be placed on how the two populations are compared. In particular, NEOs may only be compared to main-belt 'equivalents,' meaning asteroids of approximately the same size. Here, the restriction will be enforced by selecting groups of similar H-magnitudes (again

Table 3: Summary of statistical test results comparing the rotational frequencies of 'encounter' and 'non-encounter' NEOs.

n_1**range (LD)**	n_2 **range (LD)**	n_1	$\bar{f}_1$	σ_1	n_2	$\bar{f}_2$	σ_2	t *value*	$P(t)$	t **interpretation**	f *value*	$P(f)$	f **interpretation**
0 to 1	>1	41	20.7468	29.3343	42	16.4105	16.5170	0.8324	0.2038	not significant	3.1542	0.0002	very significant
0 to 2	>2	60	18.2232	25.3517	23	19.4117	19.1314	-0.2034	0.5803	not significant	1.7560	0.0726	possibly significant
0 to 3	>3	70	17.9270	24.0548	13	21.9207	22.1644	-0.5560	0.7101	not significant	1.1779	0.3992	not significant
0 to 4	>4	73	19.2946	24.6235	10	13.1354	14.9341	0.7693	0.2220	not significant	2.7186	0.0533	possibly significant
0 to 5	>5	74	19.2730	24.4549	9	12.6283	15.7484	0.7929	0.2151	not significant	2.4113	0.0914	possibly significant
0 to 6	>6	74	19.2730	24.4549	9	12.6283	15.7484	0.7929	0.2151	not significant	2.4113	0.0914	possibly significant
0 to 7	>7	77	19.5313	24.2986	6	5.9918	4.5442	1.3556	0.0895	possibly significant	28.5927	0.0007	very significant
0 to 8	>8	78	19.2849	24.2382	5	7.1276	4.0169	1.1143	0.1342	not significant	36.4099	0.0015	very significant
0 to 9	>9	78	19.2849	24.2382	5	7.1276	4.0169	1.1143	0.1342	not significant	36.4099	0.0015	very significant
0 to 10	>10	78	19.2849	24.2382	5	7.1276	4.0169	1.1143	0.1342	not significant	36.4099	0.0015	very significant

serving as a proxy measurement for size) for comparison.

In order to find the magnitude ranges that allow for MBA-equivalent comparisons, both MBAs and NEOs were grouped into 1-magnitude-wide bins and the number of objects that fell into each of these bins from 1st magnitude to 30th magnitude (leading edge) were counted. Figures 13 and 14 show how the magnitude ranges available for MBA-equivalent comparisons were found.

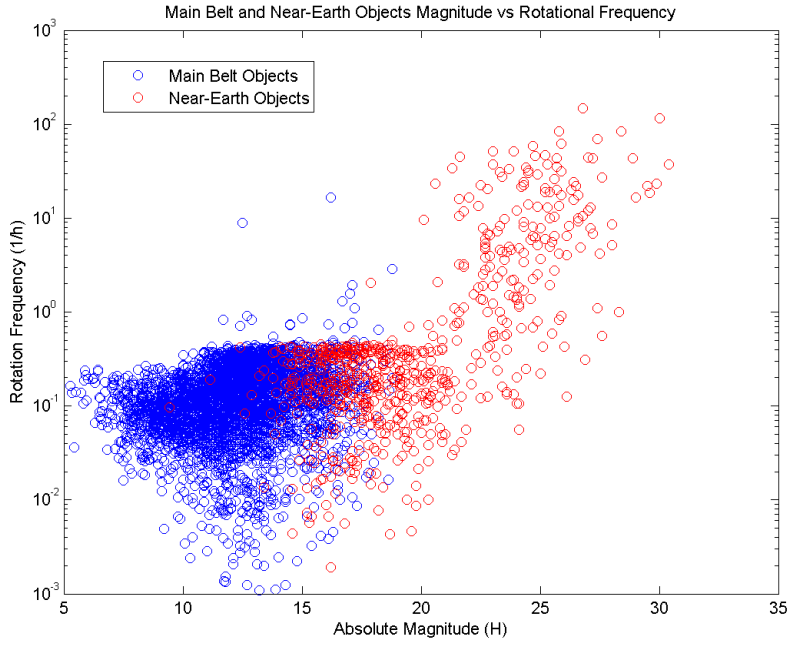

Figure 13: Plot of main belt and NEO magnitudes against rotational frequency. The magnitude ranges where both kinds of objects exist may be used for MBA-equivalent comparisons.

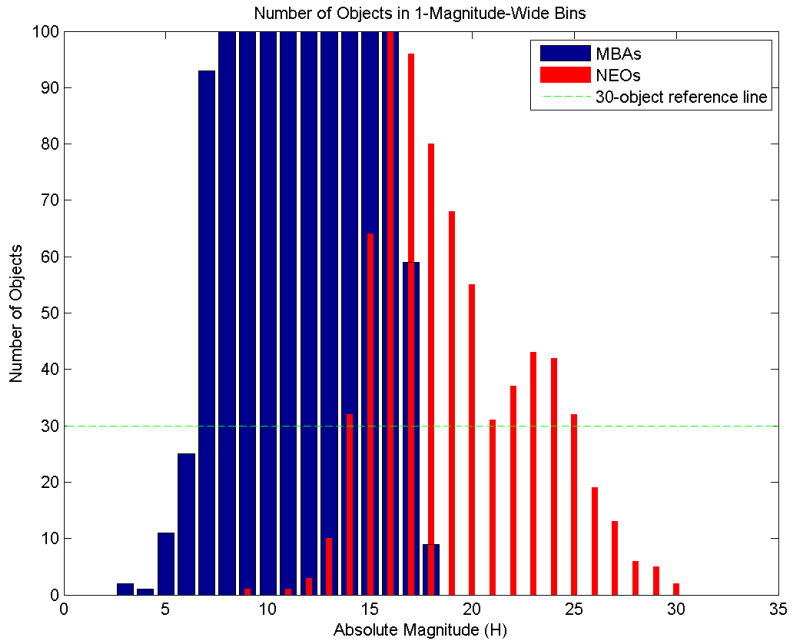

Figure 14: Number of NEOs and MBAs in 1-magnitude-wide bins (zoomed-in view). The bins' starting edges are at the absolute magnitudes indicated on the x-axis. Using 30 objects as the minimum necessary to make useful comparison, we can see that the bins starting at 14th to 17th magnitude are the only ones that can be used for comparison. The MBA counts from 8th to 16th magnitude are over 100.

After determining that with 4 comparisons are possible with 1-magnitude-wide bins, the NEOs in those bins and their MBA-equivalents were split off for statistical analysis. The counts for these bins are shown in Table 4.

Table 4: Number of objects in the NEO (n_{NEO}) and MBA (n_{MBA}) groups based on H-magnitude.

range (H-mag)	n_{MBA}	n_{NEO}
14-15	401	32
15-16	293	64
16-17	152	101
17-18	59	96

However, it is not sufficient to simply find NEO-MBA equivalents. Those within the NEO population still need to be subdivided into an 'encounter' population to

compare to the 'untouched' MBA-equivalent population. This further step significantly reduces the number of NEOs available for comparison, which makes the n_{NEO} value somewhat misleading. Figure 15 shows how the MOID values of this subset of NEOs compares to their H-magnitudes. From this, it can be seen that 1-magnitude bins will not provide enough samples for analysis, and that larger bins across both magnitude and MOID range will be required for a proper comparison with the MBA-equivalents.

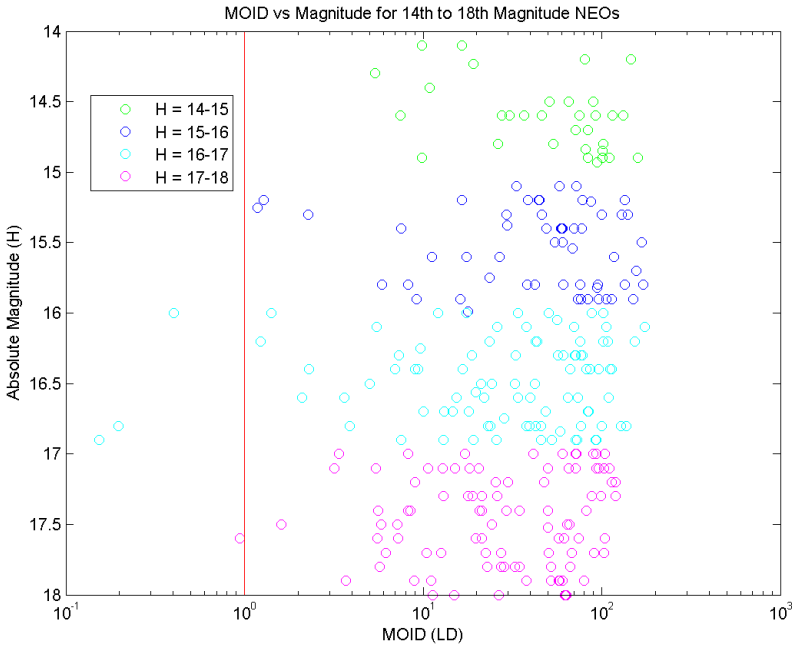

Figure 15: Plot of MOID against absolute magnitude, with the different colors representing the four MOID bins. It can be seen that there are very few NEOs in this subset with MOIDs $<$ 1 LD, which points to the necessity of combining the bins and expanding the MOID range for the 'encounter' population.

When the entire NEO subset from 14th to 18th magnitude is combined, the only 'encounter' ranges that may be compared reliably are bins that range from 0 to 7 LD to 0 to 10 LD when using a minimum of 30 objects for statistical testing. Figure 16 shows the results of the one-tailed two-sample f- and t-tests that were conducted comparing the 'encounter' NEO population with an equivalent MBA population,

while Tables 5 and 6 show the full statistics for each sample and the results that came from the tests.

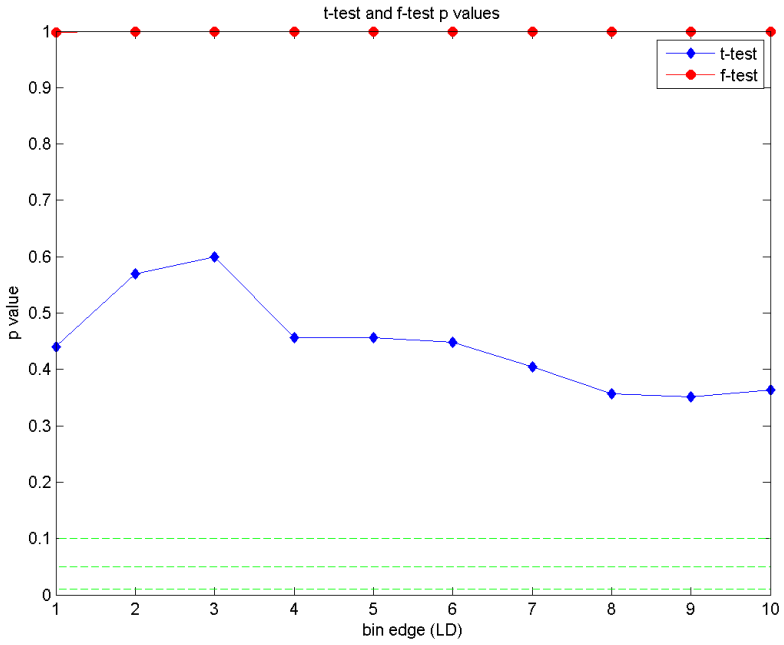

Figure 16: Results of one-tailed Student's t-tests, and one-tailed f-tests comparing rotation frequencies of NEOs and MBAs of 14th to 18th magnitude. Dashed lines represent p values of 0.1, 0.5, and 0.01, respectively.

Table 5: Summary of statistical properties of MBA-equivalents (14th to 18th magnitude).

n_{MBA}	$\bar{f}_{MBA}$	σ_{MBA}
905	0.2109	0.5637

3.4 Amplitude Analysis

In addition to the work done for rotational frequency, light curve amplitude was also examined using a similar procedure. When examining a light curve, the amplitude is the difference in magnitude between the maximum observed brightness and the minimum observed brightness in curve. Amplitude is indicative of asteroid shape,

Table 6: Summary of statistical test results comparing the rotational frequencies of 'encounter' NEOs and their MBA-equivalents. Statistics for the selection MBA-equivalent population are shown in Table 5. Note that in this table, f is frequency ($\bar{f}$ is mean frequency), while f *value* is the result obtained from the one-tailed, two-sample f-test. Given the sample sizes, only the last four samples actually give reliable statistical results.

MOID range (LD)	n_{NEO}	$\bar{f}_{NEO}$	σ_{NEO}	t *value*	$P(t)$	t **interpretation**	f *value*	$P(f)$	f **interpretation**
0 to 1	5	16.66	0.677	0.1495	0.4406	not significant	0.0278	0.9985	not significant
0 to 2	11	16.31	0.801	-0.1767	0.5701	not significant	0.0662	1.0000	not significant
0 to 3	14	16.26	0.760	-0.2539	0.6002	not significant	0.0759	1.0000	not significant
0 to 4	20	16.51	0.767	0.1107	0.4559	not significant	0.0828	1.0000	not significant
0 to 5	20	16.51	0.767	0.1107	0.4559	not significant	0.0828	1.0000	not significant
0 to 6	29	16.56	0.879	0.1296	0.4485	not significant	0.0737	1.0000	not significant
0 to 7	31	16.59	0.8743	0.2419	0.4045	not significant	0.0745	1.0000	not significant
0 to 8	37	16.56	0.917	0.3665	0.3570	not significant	0.0684	1.0000	not significant
0 to 9	44	16.64	0.900	0.3813	0.3515	not significant	0.0666	1.0000	not significant
0 to 10	50	16.53	0.950	0.3491	0.3636	not significant	0.0702	1.0000	not significant

since elongated shapes will produce larger variations in brightness when spinning along a principal axis of maximum moment of inertia. In these cases, the objects will be brighter to an observer when their elongated side is reflecting the most light towards Earth, and dimmest when their shorter sides are reflecting the most light. There may be, of course, cases of elongated asteroids spinning along their long axes, but these cases are unlikely due to the tendency of spin states to evolve towards axes of maximum moments of inertia due to their lower energy states.

To avoid a bias in the amplitude measurements (largely caused by under-sampling), amplitude bias correction was performed using the procedure described in Binzel and Sauter (1992). This procedure was used to correct for a bias introduced by possible under-sampling of light curves, which would generate a lower estimate of the amplitude. The procedure attempts to bring the amplitude estimate as close as possible to what it would be if the object was observed at a 60° phase angle. Four steps were followed to correct the amplitude bias:

1. If the asteroid has only been observed once, take that amplitude as the accepted value and assume that it was observed at a 60° phase angle because that is the statistically accepted angle (with an exception in step 4). If the asteroid has been observed multiple times, designate the minimum and maximum observed amplitudes as Min and Max, respectively.

2. If $Min - Max \leq 0.2$, then the aspect angle range is assumed to be under-sampled, and the corrected value is obtained by $(Min - Max)/2$.

3. If $Min - Max > 0.2$, then the aspect angle range is assumed to be well sampled, and the Max value is assumed to be the estimate of the amplitude at the equatorial aspect. The axis length ratios are then calculated using

$$Max = 2.5\, log(a/b) \tag{5}$$

and using laboratory results for fragment shapes,

$$c = b/\sqrt{2}. \tag{6}$$

Finally, with the ratios of $a : b : c$, the expected amplitude from a 60° aspect ratio (the bias-corrected value) is given by

$$A(\Phi = 60^\circ) = 2.5\, log\left(\frac{a}{b}\right) - 1.25\, log\left(\frac{a^2 cos^2 60^\circ + c^2 sin^2 60^\circ}{b^2 cos^2 60^\circ + c^2 sin^2 60^\circ}\right). \tag{7}$$

4. If a single observation gives an amplitude greater than 1.0 magnitude, then it is assumed that this was a rare near-equatorial observation, and Step 3 is also applied, using the observed amplitude as the Max value.

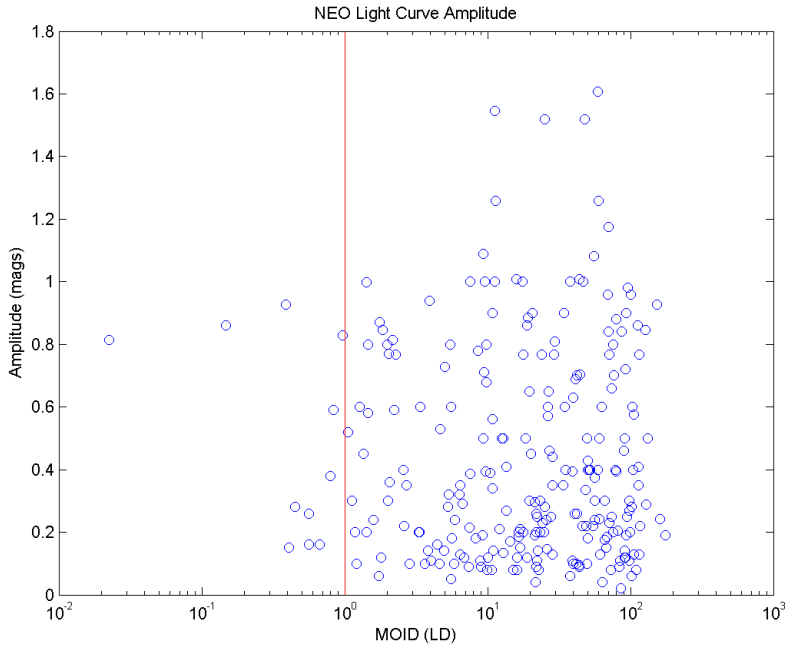

Figure 17: Bias-corrected amplitude vs. minimum orbit intersection distance for Aten, Apollo, and Amor (AAA) NEOs. The red line represents 1 LD.

Again, the property being examined was plotted against the object magnitude to check for correlation to see if the population needed to be subdivided to eliminate

a magnitude bias. In this case, however, it may be seen in Figure 18 that such a correlation does not exist for amplitude, so the kind of de-biasing used for rotational frequency is not needed.

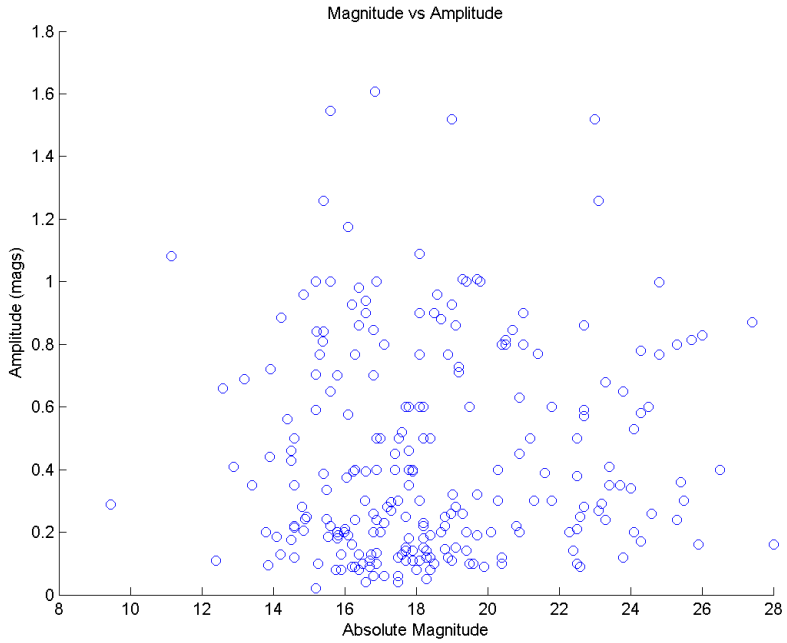

Figure 18: Plot of absolute magnitude against the light curve amplitude. In contrast to Figure 6, no noticeable correlation exists between absolute magnitude and light curve amplitude.

Next, a 30-object moving window average was applied to this sample, as shown in Figure 19. The standard deviations produced by this moving window procedure are shown in Figure 20. From these plots, it can be seen that the standard deviation is large compared to the change in the mean amplitude, and the mean amplitude never moves beyond the error bars.

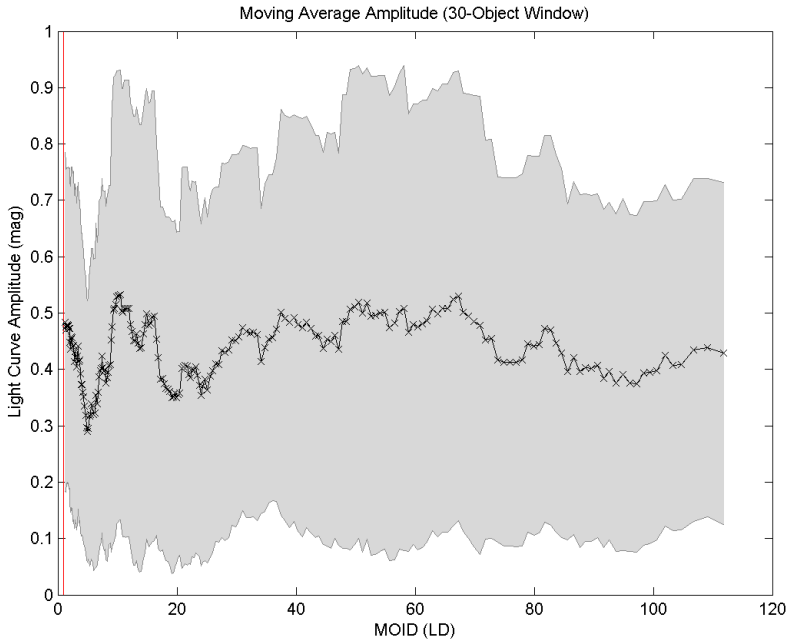

Figure 19: Moving average plot of light curve amplitude with a 1-LD reference line. Each 'x' mark represents the mean MOID of one 30-object window, and the shaded region represents one standard deviation of the mean above and below the mean value.

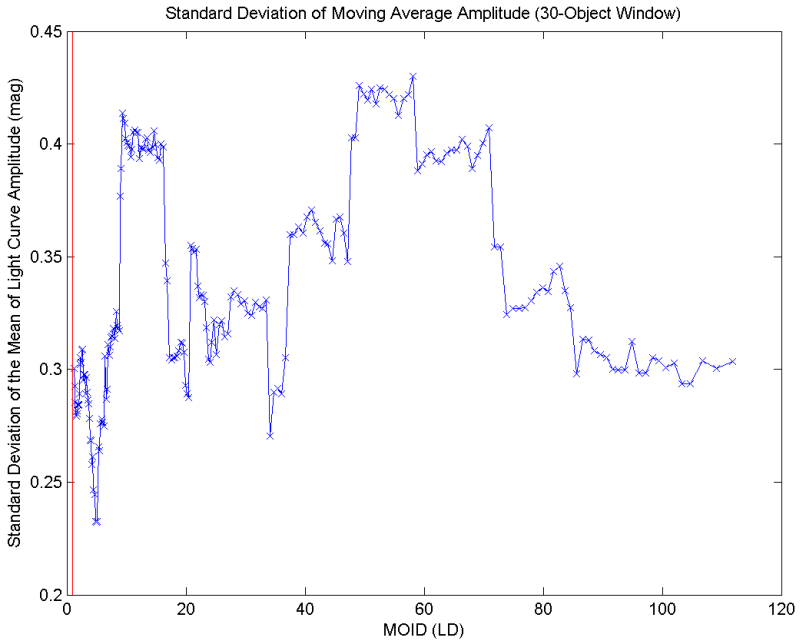

Figure 20: Plot of standard deviation of the mean of 30-object samples of objects in the magnitude range from 20 to 25. 1-LD line inserted for reference.

Finally, a two-sample one-tailed t and f-tests were conducted, using a MOID value ranging from 1 to 10 LD as the dividing value between the two samples. The sample ranging from 0 LD to the dividing MOID represents the population that is more likely to have experienced an Earth encounter, and the sample from the dividing value to 174 LD represents a population that is likely to not have experienced such an encounter. The p values produced by these tests may be seen graphically in Figure 21 and in the summary of statistics in Table 7.

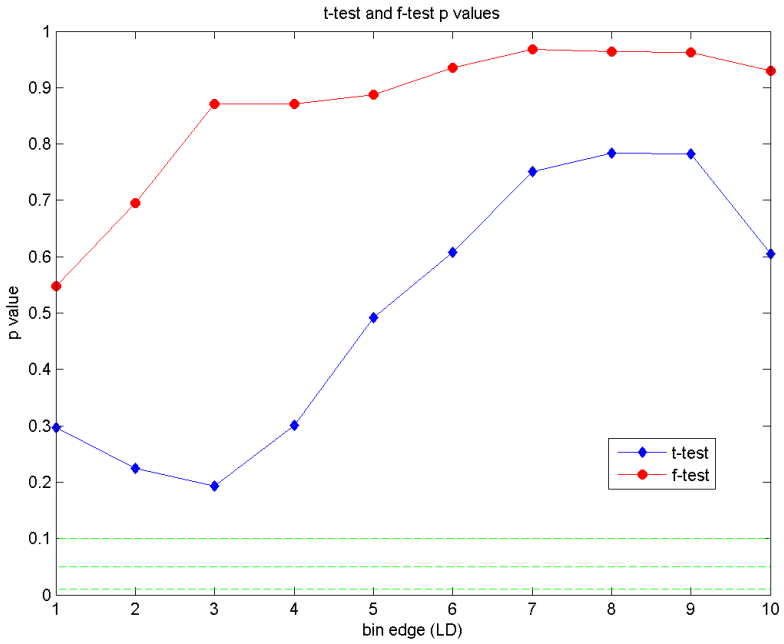

Figure 21: Results of one-tailed Student's t-tests, and one-tailed f-tests conducted for light curve amplitudes. Dashed lines represent p values of 0.1, 0.5, and 0.01, respectively.

These statistical tests show that the data do support the idea that near-Earth encounters significantly affect the shapes of NEOs.

4 Discussion

The results of the rotational frequency and light curve amplitude analysis presented in the previous section are discussed. In particular, the statistical tests are examined in relation to the hypothesis made about these properties. The tests showed statistically significant results supporting an observable effect of Earth encounters on NEO rotational frequency, did not show a similar effect on NEO light curve amplitude. The comparison between an NEO population and its MBA-equivalent also did not show an observable encounter effect, though this result is likely biased by a size/rotation correlation that affected the NEO sample being used.

Table 7: Summary of statistical test results comparing the light curve amplitudes of 'encounter' and 'non-encounter' NEOs.

n_1**range (LD)**	n_2 **range (LD)**	n_1	$\bar{A}_1$	σ_1	n_2	$\bar{A}_2$	σ_2	$t\ value$	$P(t)$	t **interpretation**	$f\ value$	$P(f)$	f **interpretation**
0 to 1	>1	11	0.4918	0.3162	235	0.4366	0.3360	0.5340	0.2969	not significant	0.8857	0.5473	not significant
0 to 2	>2	27	0.4850	0.3092	219	0.4333	0.3378	0.7573	0.2248	not significant	0.8375	0.6954	not significant
0 to 3	>3	37	0.4801	0.2914	209	0.4283	0.3416	0.8686	0.1930	not significant	0.7280	0.8717	not significant
0 to 4	>4	43	0.4638	0.2964	203	0.4344	0.3435	0.5230	0.3007	not significant	0.7446	0.8717	not significant
0 to 5	>5	48	0.4372	0.2959	198	0.4360	0.3437	0.0216	0.4914	not significant	0.7410	0.8878	not significant
0 to 6	>6	57	0.4260	0.2915	189	0.4399	0.3465	-0.2741	0.6079	not significant	0.7075	0.9349	not significant
0 to 7	>7	62	0.4112	0.2852	184	0.4446	0.3498	-0.6799	0.7514	not significant	0.6647	0.9675	not significant
0 to 8	>8	66	0.4119	0.2895	180	0.4500	0.3513	-0.7880	0.7843	not significant	0.6792	0.9636	not significant
0 to 9	>9	69	0.4095	0.2903	177	0.4465	0.3504	-0.7800	0.7819	not significant	0.6862	0.9622	not significant
0 to 10	>10	79	0.4277	0.3017	167	0.4399	0.3499	-0.2672	0.6052	not significant	0.7436	0.9293	not significant

4.1 Rotational Frequency

From Figure 12, it can be seen that the results of most the f-tests for pairs of samples divided by MOID values ranging from 1 to 10 LD all show some statistically significant difference in variance, indicating that populations of objects that have had a planetary encounter have a higher variance in rotational frequencies than those that did not. In particular, the population sizes n_1 and n_2, shown in Table 3, indicate that the most reliable test (both samples have more than 30 data points) — that of the 0 to 1 and 1 to 10 LD comparison — returns a highly significant statistical difference in variance. The fact that the t-tests do not return significant differences might be explained by the fact that planetary encounters induce largely unpredictable changes to rotational frequency, and would not necessarily shift the mean frequency one way or another even as the distribution becomes wider (Scheeres et al., 2000).

In the case of comparing the 'encounter' NEO subset to its MBA-equivalent population, all f- and t-test results returned null results. This makes sense given the subset that had to be examined. The lack of small (high-magnitude) MBAs meant that the magnitude overlap between the NEO and MBA populations was from 14th to 18th magnitude. This population's members are significantly larger than the ones examined for the intra-NEO analysis, and fall squarely within the region noted on Figure 6 as being most biased towards having lower rotational frequencies. Thus, a better comparison would require MBA data on much smaller asteroids, comparable to the 20th-30th magnitude objects used in the intra-NEO analysis. Unfortunately, data on these objects is exceeding rare due to the difficulty of detecting such small objects at main-belt distances.

4.2 Light Curve Amplitude

The data do not support the hypothesis that light curve amplitude is affected by near-Earth encounters. As noted in the hypothesis, this is a particularly difficult

phenomenon to show, since the effect only occurs with very close encounters and/or larger rubble piles. The forces of cohesion that hold asteroids together are more difficult to overcome than the forces required to torque an asteroid to a different rotational frequency, which may explain why the effect was not observed. Table 7 shows that the number of objects in the 0 to 2 LD MOID range is actually smaller than the typical minimum sample size of 30 for statistical analysis, which means that there simply is not enough information on low-MOID objects to conduct a proper analysis in the region where the amplitude effect is expected to be most easily observable. Given more samples in the very close MOID range (perhaps < 1 LD), an effect on amplitude may show up. Supplementing the existing data with incoming MANOS data would likely improve the situation of having too few data points in the close MOID range, but that is outside the scope of this project due to the MANOS data production timeline.

Part V

Conclusion

This project accomplished two primary goals: providing a free, open-source program — manosCurveFit — for light-curve fitting that was tailored for small near-Earth asteroids, and conducting an analysis of Earth encounter effects on NEO rotational frequencies and amplitudes.

The software was able to produce results that were consistent or very nearly consistent with existing light-curve fits, even when using only a small fraction of the data that was originally used to produce the accepted light-curve fits, and is currently being used by MANOS as part of its automated data reduction pipeline.

A number of improvements have been identified for manosCurveFit, largely to expand the kinds of inputs that the program can take, and partly to improve the fitting routine directly. Currently, the inputs for manosCurveFit can only be floats. It would be useful to expand the inputs to include strings, as many data files use strings to represent properties such as filter types and instruments, which currently are not accounted for in the data that is read into the program. Another improvement involves cases when data from multiple nights or telescopes are used. In these cases, an offset must be provided to each night except for one to bring all the magnitudes to the same baseline. However, in some cases, it would be easier to leave the offsets as a free parameter that can be optimized for in the same way as the other free parameters, which eliminates the need to estimate the offsets. Finally, to account for cases when multiple nights' data are used in which the nights are spread further apart (currently not the case with MANOS), phase angle considerations may be added to the fitting routine. To do this, orbital parameters must be known for the objects being analyzed. Since the fitting code is primarily operated on computers at

Lowell Observatory, it would make sense to have it poll Lowell's databases for orbital parameters once the proper infrastructure is in place for such a system.

Analysis of previous asteroid survey data showed a highly significant difference in variance in rotational frequency between NEO populations that were likely to have had an Earth encounter and those that are less likely to have had such an encounter at a dividing MOID of 1 LD. Comparison between NEOs and their MBA-equivalents did not show a significant result, likely due to the fact that the only overlapping 'equivalent' population was affected by a size/frequency bias that could not be removed from the analysis. Amplitude analysis likewise likely suffered from lack of data, as the population of NEOs with the lowest MOID values — and thus most likely to show deformation due to an encounter — was not well sampled enough to provide reliable statistical results.

Additional analysis can be done to improve the work done in this project. As previously mentioned, the dataset could be supplemented by MANOS data, which would fill in gaps in the data, particularly on high-magnitude, close-range objects. Integrated MOID would also likely prove to be a useful way to look at the data. Integrated MOID provides a more accurate picture of the likelihood of planetary encounters by integrating the orbit of an object (along with a number of virtual clones of the object offset by some distance) back in time, generally providing lower MOID bounds than an instantaneous calculation from present-day parameters would give. This method was used by Binzel et al. (2010) to show the asteroid 'freshening' effect of near-Earth encounters, and would likely prove useful here as well.

The work done on the NEO data in this project shows that there can be a noticeable effect on the spin rates of asteroids due to Earth encounters. Though the hypotheses made were based on simulations of close encounters, the simulated encounters are not the kind that were actually examined here. Previous simulation work has focused on variants of events like the breakup of Shoemaker-Levy 9 (in

extremely close encounters), or on the dynamical evolution of specific asteroids, but have not looked at longer-distance encounters that produce less dramatic changes. Modeling and analysis of a wide range of different-sized asteroids encountering the Earth at a wider range of distances may be useful in informing our understanding of the contribution of these weaker encounter effects.

References

Richard P Binzel and Linda M Sauter. Trojan, hilda, and cybele asteroids: New lightcurve observations and analysis. *Icarus*, 95(2):222–238, 1992.

Richard P Binzel, Paolo Farinella, Vincenzo Zappala, and Alberto Cellino. Asteroid rotation rates-distributions and statistics. In *Asteroids II*, volume 1, pages 416–441, 1989.

Richard P Binzel, Dmitrij F Lupishko, Mario Di Martino, Richard J Whiteley, and Gerhard J Hahn. Physical properties of near-earth objects. *Asteroids III*, 255, 2002.

Richard P Binzel, Alessandro Morbidelli, Sihane Merouane, Francesca E DeMeo, Mirel Birlan, Pierre Vernazza, Cristina A Thomas, Andrew S Rivkin, Schelte J Bus, and Alan T Tokunaga. Earth encounters as the origin of fresh surfaces on near-earth asteroids. *Nature*, 463(7279):331–334, 2010.

William F Bottke, Derek C Richardson, and Stanley G Love. Production of tunguska-sized bodies by earth's tidal forces. *Planetary and space science*, 46(2):311–322, 1998.

William F Bottke, Alberto Cellino, Paolo Paolicchi, and Richard P Binzel. An overview of the asteroids: The asteroids iii perspective. *Asteroids III*, 1:3–15, 2002.

Clark R Chapman. Asteroid collisions, craters, regoliths, and lifetimes. In *NASA Conference Publication*, volume 2053, pages 145–160, 1978.

Francesca DeMeo and Richard P Binzel. Comets in the near-earth object population. *Icarus*, 194(2):436–449, 2008.

Alan W Harris and Dmitrij F Lupishko. Photometric lightcurve observations and reduction techniques. In *Asteroids II*, volume 1, pages 39–53, 1989.

Robert Jedicke, Jeffrey Larsen, and Timothy Spahr. Observational selection effects in asteroid surveys and estimates of asteroid population sizes. *Asteroids III*, pages 71–87, 2002.

NASA JPL. Neo groups, 2014a. URL `http://neo.jpl.nasa.gov/neo/groups.html`.

NASA JPL. Absolute magnitude (h), 2014b. URL `http://neo.jpl.nasa.gov/glossary/h.html`.

David Morrison. The spaceguard survey: Report of the nasa international near-earth-object detection workshop. *NASA STI/Recon Technical Report N*, 92:34245, 1992.

Ettore Perozzi, Alessandro Rossi, and Giovanni B Valsecchi. Basic targeting strategies for rendezvous and flyby missions to the near-earth asteroids. *Planetary and Space Science*, 49(1):3–22, 2001.

Petr Pravec and Alan W Harris. Fast and slow rotation of asteroids. *Icarus*, 148(1): 12–20, 2000.

Petr Pravec, Alan W Harris, and Tadeusz Michalowski. Asteroid rotations. *Asteroids III*, 113, 2002.

Derek C Richardson, William F Bottke Jr, and Stanley G Love. Tidal distortion and disruption of earth-crossing asteroids. *Icarus*, 134(1):47–76, 1998.

Daniel J Scheeres, Steven J Ostro, Robert A Werner, Eric Asphaug, and RS Hudson. Effects of gravitational interactions on asteroid spin states. *Icarus*, 147(1):106–118, 2000.

Daniel J Scheeres, F Marzari, and A Rossi. Evolution of neo rotation rates due to close encounters with earth and venus. *Icarus*, 170(2):312–323, 2004.

Eugene M Shoemaker, JG Williams, EF Helin, and RF Wolfe. Earth-crossing asteroids: Orbital classes, collision rates with earth, and origin. *Asteroids*, 1:253–282, 1979.

Grant H Stokes, Jenifer B Evans, and Stephen M Larson. Near-earth asteroid search programs. *Asteroids III*, 1:45–54, 2002.

Yu Takahashi, Michael W Busch, and DJ Scheeres. Spin state and moment of inertia characterization of 4179 toutatis. *The Astronomical Journal*, 146(4):95, 2013.

Kevin J Walsh and Derek C Richardson. Binary near-earth asteroid formation: Rubble pile model of tidal disruptions. *Icarus*, 180(1):201–216, 2006.

Appendix

A manosCurveFit System Dependencies

This software was developed and tested on Python 2.7.1, and imports from the following typically pre-installed packages: *operator, os, time, sys*, *string*, and *cmd* and the following typically non-pre-installed packages: *lmfit, matplotlb, numpy* and *uncertainties*.

The latter set of packages are commonly used for scientific applications and stable builds should be easily found.

B manosCurveFit Input, Evaluation, and Output Methods

The software handles data input by reading text files and storing user-defined data columns as numpy arrays in a *lightCurveData* object. Evaluation is handled by the *fitData* function, which utilizes *lmfit*'s minimization routine with free parameters given as Parameter object inputs. Output is handled by the *outputResults* function, which has options to display results in various ways.

B.1 fitInfo Specification

Table 8: fitInfo keywords (all keywords are optional)

Keyword	Arguments	Meaning
FILES	integer	number of data files for this object (used as a check)
GUESS	string, then 1 or 3 integers	see Guess Specifications section, below
HARDMAXPERIOD	float or int	hard maximum period to not search above
HARDMINPERIOD	float or int	hard minimum period to not search below
OFFSET	string	starts a series of night/offset pairs used by the string specifying the dataset
ENDOFFSETS	N/A	ends the series of offsets (required if OFFSETS are used)

Example fitInfo File:

```
FILES 2
# method min max step
GUESS range 14 18 0.25
HARDMAXPERIOD 13
HARDMINPERIOD 20
OFFSET Elisa\elisa_mine_standard.txt
1 0.0
2 -0.04
3 0.464
ENDOFFSETS
OFFSET Elisa\elisa_his_standard.txt
1 -0.324
2 -0.257
3 -0.237
4 -0.194
5 -0.223
6 -0.321
7 -0.246
8 -0.372
9 -0.15
ENDOFFSETS
```

B.2 Guess Specification

Three different ways to specify initial guesses at the period value (in hours) exist.

- range (3 floats or ints) - a range of guesses will be used, following the convention

min, max, and step size

  - Example: `GUESS RANGE 0.1 5.5 0.25`

- single (1 float or int) - one initial guess will be used

  - Example: `GUESS SINGLE 2`

- None - if the GUESS line is excluded, an interval from 15 minutes to 5 times the observing window will be used (see section on fitData)

B.3 Command Line Interface

Descriptions of all command line options

- `exit` (no arguments) - exits the program

- `fit` (names of objects to be fit — separated by spaces — must match folder names in the Data directory) - runs a fit on the objects specified, regardless of whether or not they have already been processed

  - Example: `fit Martes Elisa`

- `fitAll` (no arguments, or `'redo'`) - runs fits on all objects in the Data directory that do not have an existing light curve plot; if the `'redo'` argument is provided, all plots are fitted, regardless of any existing fits

- `setFitOptions` (option and value arguments) - sets options used in the fitting routine; multiple options may be set at once

  - `minOrder` (non-negative integer argument) - sets the minimum order to be used in the Fourier fit; default is 2

- `maxOrder` (non-negative integer argument greater than minOrder) - sets the maximum order to be used in the Fourier fit; default is 6
- `timer` (boolean) - turns a fitting timer on or off, which measures the amount of time required for each fit, generally for diagnostic purposes
    - Example: `setFitOptions minOrder 3 maxOrder 5 timer true`

- `setOutputOptions` (option and boolean setting arguments) - sets options used in the program output; multiple options may be set at once; all options take booleans
    - `printReport` - whether or not to print the fitting report on the console (default is True)
    - `saveReport` - whether or not to save the fitting report to the object's directory (default is True)
    - `plotFullPeriod` - whether or not to plot the full period as determined by the model; if not, the model will only plot up to the available data (default is True)
    - `plotErrorBars` - whether or not to plot the error bars on the data (default is True)
    - `phaseFoldData` - whether or not to phase fold the data and model (default is True)
    - `plotResiduals` - whether or not to plot the residuals of the data as a subplot of the light curve (default is True)
    - `plotPeriodErrors` - whether or not to plot the mean RMS values the errors as a function of the period attempted (default is True)
    - `showPlots` - whether or not the show the plots (default is False); the plots will always be saved to the object's directory

- `showObjects` (no arguments) - lists the object subdirectories found under Data

C manosCurveFit Class and Function Specifications

C.1 The `lightCurveData` Class

class `lightCurveData`(objectName, fileNamesAndFormat[, offsetsList = None])

Creates a lightCurveData object which is used to read in and manipulate the dataset.

Parameters

- **objectName** (string) - name of the object associated with the dataset
  - Example: 'Spartacus20090130'
  - Stored in lightCurveData.name
- **fileNamesAndFormat** (dictionary of dictionaries) - names of text files to be read in, along with the associated column definitions in the data (format specification)
  - Example:

```
fileName = 'Spartacus20090130_MANOS.txt'
# list of lists specifying ['property',column] in the text file
formatSpec = [['night',0],['jd',3],['diffMag',6],['magErr',7]]
fileNamesAndFormat = {fileName:formatSpec}
```

  - Multiple key/value pairs may be used when multiple text files are to be used
  - `'jd'` (Julian date), `'diffMag'` (differential magnitude), and `'magErr'` (magnitude error) must be specified to run the program, additional properties may also be stored in the `lightCurveData` object

  - Remember that Python indexes from zero, so the left-most column in the text file is column 0
  - Any white space in the text file is considered a delimiter (leading and trailing white space is ignored)
  - Stored in lightCurveData.data

- **offsetsList** (list of dictionaries, `None` = no offsets) - offsets associated with nights in each text file
  - Example: [{1:0.0,2:-0.04,3:0.464}]
  - Key/value pairs must be int/float pairs, where the key is the night number, and the value is the offset
  - Multiple dictionaries may be used when multiple text files are to be used; when this is done, the order of these dictionaries must correspond to the order of the files names and specifications used in `fileNamesAndFormat`
  - Keys may be repeated as long as they are in different dictionaries
  - `'night'` property must be specified in the format to use offsetsList
  - **If more than one night is used for any target, all data must have associated night and offset values**
    * The only case where offsets are not necessary is if the entire dataset came from a single night

C.2 The `fitData()` Function

`fitData`(lightCurveData, fitOptions, method = None[, periodGuess = None[, hardMinPeriod = None[, hardMaxPeriod = None]]])

- **lightCurveData** (lightCurveData object)

- **fitOptions** (dictionary) - the options used in calculating the fit, as specified in `setFitOptions` (see Command Line Interface)
  - `orderMin` - minimum m value to be attempted in the Fourier model, as outlined in the Fitting Rationale section (default is 2)
  - `orderMax` - maximum m value to be attempted in the Fourier model, as outlined in the Fitting Rationale section (default is 6)
  - `timer` - whether or not to measure the amount of time it takes to fit the model (default is False)
- **method** (string) - method to be used for traversing the search space of periods: `None`, `'single'` or `'range'`; supplied by the fitInfo file, when available
  - when method is `None`, a maximum recoverable period is estimated for up to 5 times the observing window; periods are checked at 15 minute (0.25 hour) intervals; periodGuess is ignored in this case
  - when method is `single`, periodGuess must be provided as an int or a float, which serves as the only initial period used in the minimization
  - when method is `range`, periodGuess must be provided as a three-element list of `[start, stop, step]` integers or floats, which is then automatically converted into a list of initial periods for minimization
- **periodGuess** (int or float or three-element list of ints or floats) - the initial period used for minimization, given in hours; this provides a starting point for the the period parameter, which does not remain fixed during the minimization; supplied by the fitInfo file, when available
- **hardMinPeriod** (int or float) - the hard lower limit for the period fitting, no period below this value will be attempted in the evaluation; supplied by the fitInfo file, when available

- **hardMaxPeriod** (int or float) - the hard upper limit for the period fitting, no period above this value will be attempted in the evaluation; supplied by the fitInfo file, when available

Returns (bestFit, bestOrder, periodsTested, periodErrors), where bestFit is a Minimizer object, bestOrder is an int, and periodsTested and periodErrors are corresponding lists of floats.

C.3 The `outputResults()` Function

`outputResults`(fit, m, lightCurveData, outputOptions[, periodErrors = None])

- **fit** (Minimizer object) - the bestFit object returned by `fitData()`
- **m** (int) - the bestOrder returned by `fitData()`
- **lightCurveData** (lightCurveData object) - the lightCurveData object used for this run
- **outputOptions** (dictionary) - the options used in displaying and saving the results of the run, as specified in `setOutputOptions` (see Command Line Interface)
- **periodErrors** (n by 2 list of lists) - when provided, a second figure will be plotted showing the mean RMS of the residuals as a function of period